



Effects of geometrical and mechanical properties of fiber and matrix on composite fracture toughness



Yuli Chen^{a,*}, Shengtao Wang^a, Bin Liu^b, Jianyu Zhang^{a,*}

^a Institute of Solid Mechanics, Beihang University, Beijing 100191, PR China

^b AML, Department of Engineering Mechanics, Tsinghua University, Beijing 100084, China

ARTICLE INFO

Article history:

Available online 13 December 2014

Keywords:

Nano-composites
Ultrathin fibers
Nanotubes
Fracture toughness
Fiber bridging

ABSTRACT

Composites reinforced by thinner fibers are intensively studied in recent years and expected to have better mechanical properties. With development of nanotechnology, the diameter of fiber can be as thin as several nanometers, such as nanofibers and nanotubes. Then, do these thinner fibers definitely result in composites with better mechanical properties? In this paper, the toughening effect of reinforcing fibers in composites is investigated based on the three-level failure analysis model. It is found that thinner reinforcing fibers do not definitely confer better fracture toughness on composites. The optimal fiber diameter is that making the failure mode just in the transition from fiber pull-out to fiber break, which is about 2–6 nm for carbon nanotubes and around 100 nm for carbon nanofibers. In addition, the effects of fiber, matrix and interface properties are all investigated, and their analytical optimal values are obtained and summarized in a table, which provides important reference for advanced composites design.

© 2014 Elsevier Ltd. All rights reserved.

1. Introduction

Fiber reinforced composites have been widely used in various fields, especially in aerospace, military and automotive industries. With the development of nanomaterials, the fiber-type reinforcements with diameters as thin as several nanometers, such as nanotubes (NTs) and nanofibers (NFs), are increasingly used in advanced composites for better mechanical, electrical, optical and chemical properties [1–5].

As thin, strong and multifunctional reinforcements, NFs/NTs have drawn extensive attentions of researches. Taking carbon nanotubes (CNTs) [6–11] for example, their Young's modulus and strength are up to 1 TPa and 100 GPa, respectively [9–11], and their diameter typically ranges from 0.8 nm to 2 nm for single-wall CNTs (SWCNTs) and from 5 nm to 20 nm for multi-wall CNTs (MWCNTs) [9]. Tremendous efforts have been done to investigate the mechanical [12–23], electrical [12–15,24] and thermal [15,25–27] properties of CNT-reinforced composites. Thereinto, a large part of the works focuses on the toughening effect of CNT-reinforced composites. Experiments have shown large scattering and even opposite results in the improvement in fracture toughness by the CNTs,

ranging from –10% to 4080% [16–23]. The large scattering of experimental data is mainly attributed to CNT/matrix interface [23] as well as the content and dispersion of CNTs [19,23]. In order to make deeper investigations for a better view to the toughness of CNT reinforced composites, theoretical and simulation studies have also been carried out [28–40]. Chen et al. [30] studied the toughness of composites reinforced by curved CNTs with a statistical distribution of strength, and suggested that increasing CNT curvature could reduce toughness of nano-composites depending on chosen parameters such as interfacial friction properties, and nanotube and matrix modulus. Pavia and Curtin [31] investigated the effect of wave, finite-length nanofibers on the tensile strength and fracture work of ceramic matrix. They have considered many factors to make their model close to the real problem, including interfacial friction and sliding [32–34], strength distribution, and curvature and length of nanofibers. They revealed an optimal region of morphology that maximizes composite strength and toughness. Chen et al. [35,36] developed a three-level failure analysis model to investigate the interfacial effect on the fracture toughness enhancement of CNTs. They found that neither longer reinforced CNTs nor stronger CNT/matrix interfaces can definitely lead to better fracture toughness of these composites. Furthermore, the optimal interfacial strength and the optimal CNT length are those making the failure mode just in the transition from CNT pull-out to CNT break.

* Corresponding authors. Tel.: +86 (0) 10 8231 8410; fax: +86 (0) 10 8233 9228 (Y. Chen). Tel.: +86 (0) 10 8233 8663; fax: +86 (0) 10 8233 9228 (J. Zhang).

E-mail addresses: yulich@buaa.edu.cn (Y. Chen), jyzhang@buaa.edu.cn (J. Zhang).

However, an important question arises: do thinner fibers definitely result in composites with better mechanical properties? Usually, thinner fibers are supposed to confer better mechanical properties on composites due to their higher specific interfacial area and larger aspect ratio [45,41–45]. But when the research scope extends to nano-composites and the concept of fiber extends to nanofibers and nanotubes, the effect of fiber diameter on the mechanical properties of composites remains unrevealed. Besides, another similar question is: do stiffer fibers definitely result in composites with better mechanical properties? It is of great importance to reveal the effect of fiber stiffness on the mechanical properties of composites. This paper aims to provide answers to these questions by investigating the effects of fiber diameter and fiber stiffness as well as other fiber, matrix and interface properties on the composite fracture toughness.

2. Fracture toughness enhancement

As reviewed above, there are already a large amount of theoretical models for the fracture toughness of NFs/NTs reinforced composites [28–40]. However, a simple analytical solution is desired by material researchers for convenient applications in practical composites. Chen et al.'s study [35] provides a simple analytical expression for the fracture toughness enhanced by bridging CNTs in composites. Their theoretical outcomes agree well with atomic simulations [35] and the degraded result of Pavia and Curtin's model [32], and have been validated by experiments [37,38]. So Chen et al.'s model is adopted in this paper.

Following Chen et al.'s three-level failure analysis model [35], in composites with macroscopic cracks, high strength reinforcing fibers can retard crack propagation, and a fracture zone bridged by fibers is formed at the crack tip, as shown in Fig. 1(a). This toughening effect of bridging fibers is equivalent to that of nonlinear springs connecting the upper and lower crack surfaces, as shown in Fig. 1(b). In this level, the fracture toughness enhancement of the bridging fibers can be obtained by fracture mechanics provided that the force-displacement relation for these springs is known. In order to attain the constitutive relation of the springs, the pulling force F and pull-out displacement δ of a single fiber are studied, as shown in Fig. 1(c). In this level, it is well acknowledged that the two typical failure modes are interfacial debonding and fiber break, and the F – δ curve can be solved by mesomechanics analysis [46–51]. The F – δ curve and failure mode depend on the interfacial interactions, such as atomic bond properties for NF/NT reinforced composites and cohesive forces for fiber–matrix material systems, as shown in Fig. 1(d). Therefore, the fiber reinforced composites have three failure mode levels: a bond break at the atomistic level, fiber failure mode at the mesoscopic level and

macroscopic crack propagation at the macroscopic level. It should be noted that the fibers in Fig. 1 are all well oriented because experimental observations on the crack tip of CNT reinforced composite shows that most bridging CNTs are perpendicular to crack face due to the pulling stress [52] although they are actually distributed randomly in the matrix. So the model in Fig. 1 can be extended for composites with randomly distributed fibers as well. In this paper, we will focus on the oriented fibers in order to establish simple and practical analytical formulae for the effects of fiber and matrix properties.

In atomistic level, a bond break occurs when the relative displacement between the fiber and the matrix Δu reaches the critical shear displacement δ_b , which depends only on the type of functionalization bond at the interface, and the corresponding interface strength τ_b also depends on the interface bond density. The interface shear stress τ is assumed to be proportional to the relative displacement Δu , i.e.,

$$\tau(x) = k\Delta u(x) = k[u_m(x) - u_f(x)] \quad (1)$$

where $k = \tau_b/\delta_b$ is the shear stiffness of the interface, $u_m(x)$ and $u_f(x)$ are the axial displacements of the matrix and the fiber respectively, and x is the coordinate along the axial direction.

Supposing the fiber and the matrix are both linear elastic, with the balance conditions of the fiber and the matrix, the shear stress distribution can be derived as [35,48]

$$\tau(x) = \frac{F}{\pi d_f^2} \sqrt{\frac{\tau_b}{4E_f \delta_b d_f \left(1 + \frac{E_f c_f}{E_m(1-c_f)}\right)}} \cdot \frac{\frac{E_f c_f}{E_m(1-c_f)} \cosh\left(x \sqrt{\frac{4\tau_b}{E_f \delta_b d_f} \left(1 + \frac{E_f c_f}{E_m(1-c_f)}\right)}\right) + \cosh\left[(x-L) \sqrt{\frac{4\tau_b}{E_f \delta_b d_f} \left(1 + \frac{E_f c_f}{E_m(1-c_f)}\right)}\right]}{\sinh\left(L \sqrt{\frac{4\tau_b}{E_f \delta_b d_f} \left(1 + \frac{E_f c_f}{E_m(1-c_f)}\right)}\right)} \quad (2)$$

where E_f and E_m are the Young's modulus of the fiber and the matrix respectively, c_f is the area fraction of fibers on the crack face and represents fiber volume fraction in composites, F is the pulling force, L is the embedded length and d_f is the fiber diameter.

The distribution of the axial normal stress in the fiber can also be derived as

$$\sigma(x) = \frac{4}{\pi d_f^2} \left[F - \int_0^x \pi d_f \tau(x) dx \right] \quad (3)$$

The two main fiber-level failure modes are usually interfacial debonding and fiber break. Fiber break occurs when the maximum axial normal stress reaches fiber strength σ_f^b . When the maximum shear stress reaches the interface strength τ_b , the interfacial chemical bonds break, and the fiber is pulled out. Thus, the debonding/breaking critical condition can be established.

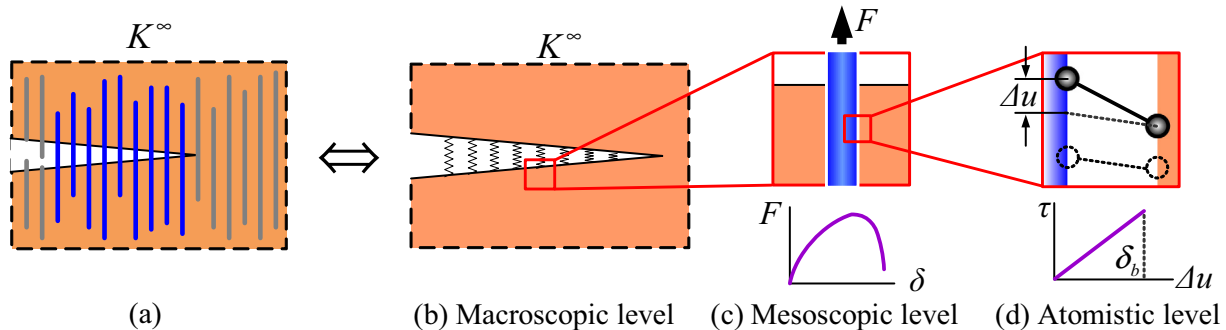


Fig. 1. Hierarchical failure analysis models: (a) fracture zone bridged with fibers at the crack tip; (b) macroscopic-level model with equivalent bridging nonlinear springs; (c) mesoscopic-level model to obtain the force-displacement relation of equivalent nonlinear spring; (d) atomistic-level failure model for characterizing fiber/matrix interfacial bond breaking.

For composites with the matrix soft enough that satisfy the condition of $E_m < c_f E_f / (1 - c_f)$, such as polymer matrix composites, the critical condition can be expressed as

$$CRI_S = \frac{\sigma_f^b}{\sqrt{\frac{4E_f \tau_b \delta_b}{d_f} \left(\frac{c_f E_f}{(1-c_f)E_m} + 1 \right)}} \frac{\frac{c_f E_f}{(1-c_f)E_m} \cosh \left(L \sqrt{\frac{4\tau_b}{E_f \delta_b d_f} \left(\frac{c_f E_f}{(1-c_f)E_m} + 1 \right)} \right) + 1}{\sinh \left(L \sqrt{\frac{4\tau_b}{E_f \delta_b d_f} \left(\frac{c_f E_f}{(1-c_f)E_m} + 1 \right)} \right)} \quad (4)$$

If $CRI_S > 1$, the dominant failure mode is interface failure with steady debonding between fiber and matrix from the inside end of fiber, named as failure mode I. And $CRI_S < 1$ indicates the failure is dominated by fiber break, named as failure mode II.

Therefore, based on fracture mechanics [53,54], for composites with soft matrix, the fracture toughness enhancement ΔK_S can be expressed analytically as [35]

$$\Delta K_S = \begin{cases} \frac{E_m \delta_b (1-c_f) \sqrt{\frac{2\tau_b \delta_b}{\pi E_f d_f} \left(\frac{c_f E_f}{(1-c_f)E_m} + 1 \right)}}{\eta K_{IC} \sqrt{1 - \left(\frac{1-c_f E_m}{c_f E_f} \right)^2}} \left\{ \pi - 2 \arctan \left[\frac{1 + \frac{1-c_f E_m}{c_f E_f} \cosh \left(L \sqrt{\frac{4\tau_b}{E_f \delta_b d_f} \left(\frac{c_f E_f}{(1-c_f)E_m} + 1 \right)} \right)}{\sinh \left(L \sqrt{\frac{4\tau_b}{E_f \delta_b d_f} \left(\frac{c_f E_f}{(1-c_f)E_m} + 1 \right)} \right) \sqrt{1 - \left(\frac{1-c_f E_m}{c_f E_f} \right)^2}} \right] \right\} & \text{if } CRI_S > 1 \text{ (Interfacial debonding)} \\ \frac{c_f (\sigma_f^b)^2}{\eta K_{IC}} \sqrt{\frac{\delta_b d_f}{2\pi E_f \tau_b \left(\frac{c_f E_f}{(1-c_f)E_m} + 1 \right)}} \cdot \frac{\cosh \left(L \sqrt{\frac{4\tau_b}{E_f \delta_b d_f} \left(\frac{c_f E_f}{(1-c_f)E_m} + 1 \right)} \right) + \frac{c_f E_f}{1-c_f E_m}}{\sinh \left(L \sqrt{\frac{4\tau_b}{E_f \delta_b d_f} \left(\frac{c_f E_f}{(1-c_f)E_m} + 1 \right)} \right)} & \text{if } CRI_S < 1 \text{ (Fiber break)} \end{cases} \quad (5)$$

where K_{IC} is the fracture toughness of pure matrix material and $\eta = 2\sqrt{2}(1 - \nu_m^2)/(E_m \sqrt{\pi})$ depends only on Young's modulus and Poisson's ratio of the matrix ν_m .

For composites with the matrix hard enough that satisfy the condition of $E_m \geq c_f E_f / (1 - c_f)$, such as composites with metal and ceramic matrix, the critical condition that judges the fiber-level failure mode can be expressed as

$$CRI_H = \frac{\sigma_f^b}{\sqrt{\frac{4E_f \tau_b \delta_b}{d_f} \left(\frac{c_f E_f}{(1-c_f)E_m} + 1 \right)}} \frac{\frac{c_f E_f}{(1-c_f)E_m} + \cosh \left(L \sqrt{\frac{4\tau_b}{E_f \delta_b d_f} \left(\frac{c_f E_f}{(1-c_f)E_m} + 1 \right)} \right)}{\sinh \left(L \sqrt{\frac{4\tau_b}{E_f \delta_b d_f} \left(\frac{c_f E_f}{(1-c_f)E_m} + 1 \right)} \right)} \quad (6)$$

If $CRI_H > 1$, the dominant failure mode is interface failure with unsteady debonding between fiber and matrix from the outside end of fiber, named as failure mode III. If $CRI_H < 1$, the failure is dominated by fiber break.

For composites with hard matrix, the fracture toughness enhancement ΔK_H can be expressed as [36]

$$\Delta K_H = \begin{cases} \frac{c_f \delta_b \sqrt{\frac{8E_f \tau_b \delta_b}{\pi d_f} \left(\frac{c_f E_f}{(1-c_f)E_m} + 1 \right)}}{\eta K_{IC}} \frac{\sinh \left(L \sqrt{\frac{4\tau_b}{E_f \delta_b d_f} \left(\frac{c_f E_f}{(1-c_f)E_m} + 1 \right)} \right)}{\cosh \left(L \sqrt{\frac{4\tau_b}{E_f \delta_b d_f} \left(\frac{c_f E_f}{(1-c_f)E_m} + 1 \right)} \right) + \frac{c_f E_f}{1-c_f E_m}} + \int_{\delta_b}^{\delta_{\max}} \sqrt{\frac{2}{\pi}} \frac{2c_f F_{\text{soften}}(\delta)}{\eta K_{IC} \frac{\pi d_f^2}{4}} d\delta & \text{if } CRI_H > 1 \text{ (Interfacial debonding)} \\ \frac{c_f (\sigma_f^b)^2}{\eta K_{IC}} \sqrt{\frac{d_f \delta_b}{2\pi E_f \tau_b \left(\frac{c_f E_f}{(1-c_f)E_m} + 1 \right)}} \frac{\cosh \left(L \sqrt{\frac{4\tau_b}{E_f \delta_b d_f} \left(\frac{c_f E_f}{(1-c_f)E_m} + 1 \right)} \right) + \frac{c_f E_f}{1-c_f E_m}}{\sinh \left(L \sqrt{\frac{4\tau_b}{E_f \delta_b d_f} \left(\frac{c_f E_f}{(1-c_f)E_m} + 1 \right)} \right)} & \text{if } CRI_H < 1 \text{ (fiber break)} \end{cases} \quad (7)$$

In the first expression of Eq. (7), the function $F_{\text{soften}}(\delta)$ is solved from the function of $\delta(F)$ as

$$\delta(F) = \delta_b + \left\{ L - \sqrt{\frac{E_f d_f \delta_b}{4\tau_b \left(1 + \frac{c_f E_f}{(1-c_f)E_m} \right)}} \ln \left[\frac{F + \sqrt{F^2 + \left(\frac{1-c_f E_m}{c_f E_f} \right)^2 \left(\frac{\tau_b \delta_b E_f \pi^2 d_f^2}{4} \left(1 + \frac{c_f E_f}{(1-c_f)E_m} \right) - F^2 \right)}}{\frac{1-c_f E_m}{c_f E_f} \left(E_f \pi d_f^2 \sqrt{\frac{\tau_b \delta_b}{4E_f d_f} \left(1 + \frac{c_f E_f}{(1-c_f)E_m} \right) - F} \right)} \right] \right\} \left(\frac{4F}{E_f \pi d_f^2} \right) \quad (8)$$

The upper limit of the integral in Eq. (7), δ_{\max} , is determined by $\partial \delta(l)/\partial l = 0$, where $\delta(l)$ is given as

$$\delta(l) = \delta_b + (L - l) \left(\sqrt{\frac{4\tau_b \delta_b}{E_f d_f} \left(1 + \frac{c_f E_f}{(1-c_f)E_m} \right)} \times \frac{\sinh \left(l \sqrt{\frac{4\tau_b}{\delta_b d_f} \left(\frac{c_f E_f}{(1-c_f)E_m} + 1 \right)} \right)}{\cosh \left(l \sqrt{\frac{4\tau_b}{\delta_b d_f} \left(\frac{c_f E_f}{(1-c_f)E_m} + 1 \right)} \right) + \frac{c_f E_f}{(1-c_f)E_m}} \right) \quad (9)$$

3. Effect of fiber diameter on fracture toughness

A typical idea about the diameter effect on the fiber reinforced composites is that thinner fibers can toughen the composites better due to their large specific interface area and accordingly stronger bonding between fibers and matrix. However, when the research scope extends to nano-composites, it should be questioned that whether or not the diameter effect follows the same rule. This section will reveal the diameter effect on the fracture toughness of NFs/NTs reinforced composites.

3.1. Effect of fiber diameter d_f

With given volume fraction, interface properties and materials for matrix and fibers, it can be observed easily from Eqs. (4) and (6) that both CRI_S and CRI_H are monotone-increasing functions of the fiber diameter d_f , ranging from 0 to infinity, which means the failure mode of composites with fibers thin enough is definitely fiber break and that of composites with fibers thick enough is definitely interfacial debonding. Thus, when decreasing the fiber diameter d_f , the failure mode can change from interfacial debonding to fiber break, for composites with both soft matrix and hard matrix. This theoretical result is consistent with the widely-accepted knowledge. The load-bearing capacity of fiber is proportional to d_f^2 while the load-bearing capacity of the interface is in direct proportion to d_f . Therefore, the fiber is relatively stronger than the interface when the fiber diameter d_f is large, and the failure mode is interfacial debonding. Conversely, the fiber diameter d_f can certainly reach a value small enough to make the fiber relatively weaker than the interface at which the failure mode becomes fiber break.

For composites with soft matrix ($E_m < c_f E_f / (1 - c_f)$), it can be seen clearly from the analytical Eq. (5) that ΔK_S increases monotonously with increasing d_f for fiber break case and decreases monotonously with increasing d_f for interfacial debonding case. Therefore, when decreasing the fiber diameter d_f from a very large value to a very small value, the failure mode is first interfacial debonding, the fracture toughness enhancement ΔK_S increases, and then at the critical point, $CRI_S = 1$, the failure mode changes to fiber break, and if the fiber diameter d_f is decreased further, the fracture toughness enhancement ΔK_S decreases. Thus the optimal fracture toughness enhancement is obtained when the failure mode is just in the transition from interfacial debonding to fiber break, as shown in Fig. 2(a). Here, the SWCNT reinforced epoxy matrix composite is adopted as an example to present the $\Delta K_S - d_f$ relation, and our studies have proved all the cases with $E_m < c_f E_f / (1 - c_f)$ present similar curves to those shown in Fig. 2(a). For the case shown in Fig. 2(a), the interfacial shear strength τ_b and the critical shear displacement δ_b are obtained from atomistic simulation as 6.0 GPa and 0.318 nm, respectively. The matrix modulus $E_m = 3.5$ GPa, CNT modulus $E_f = 700$ GPa, CNT strength $\sigma_f^b = 50$ GPa, CNT length $L = 20$ nm and CNT volume fraction $c_f = 1.0\%$, which are all within the reported ranges [9–11]. The fracture toughness enhancement is normalized as $\Delta \hat{K} = \Delta K_S \cdot \eta K_{IC} / (c_f \sigma_f^b \delta_b)$, and the CNT diameter is normalized by its critical value at which the transition between failure modes occurs.

For composites with hard matrix ($E_m \geq c_f E_f / (1 - c_f)$), the DWCNT reinforced ceramic matrix composite is used as an example to present the relation between fracture toughness enhancement ΔK_H and fiber diameter d_f , which is solved numerically

from Eq. (7) and shown in Fig. 2(b). It should be noted that our studies have proved all the cases with $E_m \geq c_f E_f / (1 - c_f)$ present similar curves to those shown in Fig. 2(b). For the case shown in Fig. 2(b), the interfacial shear strength τ_b and the critical shear displacement δ_b are 6.0 GPa and 0.318 nm respectively, according to the results of atomistic simulations. The matrix modulus $E_m = 300$ GPa, CNT modulus $E_f = 400$ GPa, CNT strength $\sigma_f^b = 30$ GPa, CNT length $L = 10$ nm and CNT volume fraction $c_f = 1.0\%$, which are all within the reported ranges [9–11]. The fracture toughness enhancement is normalized as $\Delta \hat{K} = \Delta K_H \cdot \eta K_{IC} / (c_f \sigma_f^b \delta_b)$, and the CNT diameter is normalized by its critical value at which the transition between failure modes occurs. Similar to the case of soft matrix, reducing the fiber diameter d_f from a value large enough can increase the fracture toughness enhancement ΔK_H until d_f reaches the critical condition of $CRI_H = 1$, at which the failure mode changes from interfacial debonding to fiber break, and then further reducing d_f results in decrease of ΔK_H . The optimal fracture toughness enhancement is reached when the failure mode just in the transition. It should be noted that the fracture toughness enhancement for hard matrix, ΔK_H , is much higher than that for soft matrix, ΔK_S , in the interfacial debonding mode, because the debonding stage is much longer for hard matrix according to Eq. (8), in which the debonding failure begins from outside of the fibers. So fibers can toughen hard matrix better than soft matrix.

For both cases, when the failure mode is fiber break, the fracture toughness enhancement is determined by the load-bearing capacity of fiber, so thicker fibers with stronger load-bearing capacity are better for improving fracture toughness of composites. Contrarily, when the failure mode is interfacial debonding, the fiber load-bearing capacity is large enough and the interface load-bearing capacity becomes crucial, thinner fibers with larger specific surface area can make a better use of interface strength, and hence enhance fracture toughness better.

3.2. The optimal fiber diameters

Above analysis indicates that thinner fiber cannot definitely toughen the composites better. The optimal fiber diameter is that making the failure mode just in the transition from fiber pull-out to fiber break, and can be solved from the critical conditions of $CRI_S = 1$ and $CRI_H = 1$ for composites with soft and hard matrix, respectively.

The interfacial length L is generally much larger than the fiber diameter d_f and the critical interfacial shear displacement δ_b , which is on the same order of the critical bond length. Therefore, it is reasonable to suppose $L / \sqrt{\delta_b d_f} \rightarrow \infty$, and thus the optimal fiber diameter can be solved analytically from the critical conditions of failure mode as

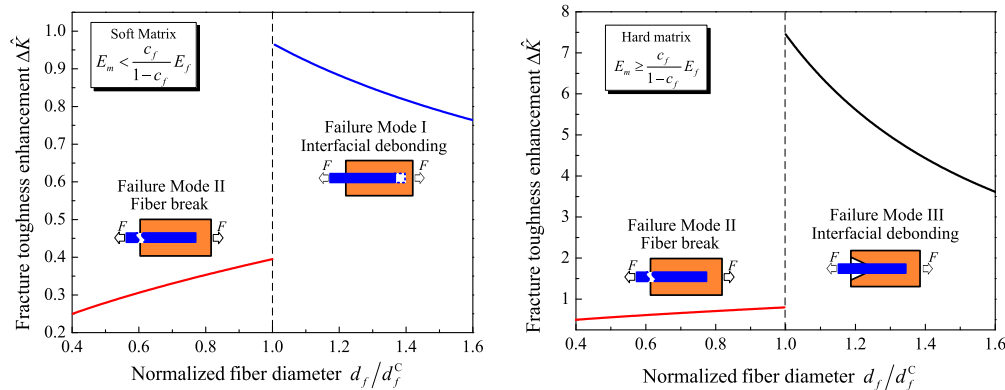


Fig. 2. Effect of fiber diameter on the fracture toughness enhancement: (a) soft matrix ($E_m < c_f E_f / (1 - c_f)$); (b) hard matrix ($E_m \geq c_f E_f / (1 - c_f)$).

$$d_f^c = \begin{cases} \frac{4\tau_b\delta_b(1-c_f)E_m[c_fE_f+(1-c_f)E_m]}{E_f(c_f\sigma_f^b)^2} & E_m < \frac{c_f}{1-c_f}E_f \\ \frac{4\tau_b\delta_bE_f[c_fE_f+(1-c_f)E_m]}{E_m(1-c_f)(\sigma_f^b)^2} & E_m \geq \frac{c_f}{1-c_f}E_f \end{cases} \quad (10)$$

If the fiber diameter $d_f > d_f^c$, the failure mode is interfacial debonding, and if $d_f < d_f^c$, the failure mode is fiber break. Accordingly, on the assumption of $L/\sqrt{\delta_b d_f} \rightarrow \infty$ the optimal fracture toughness enhancements can be obtained respectively from the simplification of Eqs. (5) and (7) as

$$\Delta K_S^{\text{optimal}} = \Delta K_S|_{d_f=d_f^c} = \frac{c_f\delta_b\sigma_f^b}{\eta K_{IC}\sqrt{2\pi}\sqrt{1-\left[\frac{(1-c_f)E_m}{c_fE_f}\right]^2}} \left\{ \pi - 2\arctan \frac{1}{\sqrt{\left[\frac{c_fE_f}{(1-c_f)E_m}\right]^2 - 1}} \right\} \quad (11)$$

$$\Delta K_H^{\text{optimal}} = \Delta K_H|_{d_f=d_f^c} = \sqrt{\frac{2}{\pi}} \frac{c_f\delta_b\sigma_f^b}{\eta K_{IC}} + \int_{\delta_b}^{\delta_{\max}|_{d_f=d_f^c}} \frac{c_f\sqrt{\frac{2}{\pi}}[(1-c_f)E_m(\sigma_f^b)^2]^2 F_{\text{soften}}(\delta)|_{d_f=d_f^c}}{2\pi\eta K_{IC}\{\tau_b\delta_bE_f[c_fE_f+(1-c_f)E_m]\}^2} d\delta \quad (12)$$

3.3. The optimal fiber diameters for typical composites

For typical fiber reinforced composites, the optimal fiber diameters d_f^c are calculated by Eq. (10) and listed in Table 1. In Table 1, the material properties of fiber and matrix are in the range reported in relative articles [1–11]. The interface parameters τ_b and δ_b for CNT and carbon nanofiber (CNF) reinforced composites are determined by atomic simulation as 6.0 GPa and 0.318 nm, respectively, which are close to the values suggested by Pavia and Curtin [33].

For composites reinforced by CNTs, Table 1 suggests that the optimal fiber diameter is about 2–6 nm, depending on the CNT types and volume fractions. The diameter of CNTs usually ranges from 0.8 nm to 20 nm [9], with the optimal value included. For CNFs, the strength and Young's modulus are 1–8 GPa and 100–500 GPa, respectively [55–57], and the optimal fiber diameter is thus around one hundred nanometers, which is in the range of the diameters of typical CNFs (50–200 nm).

So the optimal fiber diameter can be reached for CNT/CNF reinforced composites when reducing fiber diameters. If the diameter is lower than its optimal value, reducing fiber diameter leads to a decline in fracture toughness of the composites, which is opposite to the traditional concept about the diameter effect. Therefore, selecting a proper fiber diameter is important for improving fracture toughness of composites.

4. Effect of fiber stiffness on fracture toughness

Mesomechanics of composites indicates that stiffer fibers lead to higher effective stiffness of the composites [58], which

Table 1
The optimal fiber diameters for typical fiber reinforced composites.

Composites	$c_f/\%$	E_f/GPa	σ_f^b/GPa	E_m/GPa	d_f^c/nm
SWCNT/epoxy	0.5	700	50	3.5	4.24
SWCNT/ceramic	0.5	700	50	300	2.16
MWCNT/epoxy	1.0	400	30	3.5	5.48
MWCNT/ceramic	1.0	400	30	300	3.44
CNF/epoxy	1.5	300	5	3.5	124
CNF/ceramic	1.5	300	5	300	93.0

c_f : fiber volume fraction, E_f : fiber modulus, σ_f^b : fiber strength, E_m : matrix modulus, d_f^c : the critical fiber diameter.

encourages researchers to prepare fibers with high modulus. However, researchers found that flexible fibers are much better than stiff fibers in improving impact strength of fiber-reinforced composites [59]. Then, to make fiber stiffer or more flexible, which is the better way to improve the fracture toughness of composites? This section will try to answer this question. In this paper the stiffness of fiber is characterized by its axial Young's modulus E_f .

4.1. Effect of fiber modulus E_f on fracture toughness enhancement ΔK

The effect of fiber modulus E_f on the fracture toughness can also be observed from Eqs. (4)–(7). For the composites with certain matrix material and fiber volume fraction, when E_f increases from a value small enough ($E_f \leq (1-c_f)E_m/c_f$) to a value large enough ($E_f > (1-c_f)E_m/c_f$), the type of composites changes from “hard matrix” to “soft matrix”. Accordingly the fracture toughness enhancement should be calculated by Eq. (7) for the former case and Eq. (5) for the latter case, and the corresponding failure modes are determined by Eqs. (6) and (4), respectively.

As discussed in Section 3.2, it is reasonable to suppose $L/\sqrt{\delta_b d_f} \rightarrow \infty$, so Eqs. (4) and (6) can be simplified as

$$\text{CRI}_S = \frac{c_f\sigma_f^b}{(1-c_f)E_m\sqrt{\frac{4\tau_b\delta_b}{d_f}\left[\frac{c_f}{(1-c_f)E_m} + \frac{1}{E_f}\right]}} \quad (13)$$

$$\text{CRI}_H = \frac{\sigma_f^b}{E_f\sqrt{\frac{4\tau_b\delta_b}{d_f}\left[\frac{c_f}{(1-c_f)E_m} + \frac{1}{E_f}\right]}} \quad (14)$$

It can be found from Eq. (13) that CRI_S increases monotonously with the increase of E_f , and approaches asymptotically to its upper bound

$$\text{CRI}_S^{\text{up}} = \sqrt{\frac{c_f d_f (\sigma_f^b)^2}{4(1-c_f)E_m\tau_b\delta_b}} \quad (15)$$

And CRI_S can reach its minimum value when E_f reaches its minimum value of “soft matrix” case, which is $E_f = (1-c_f)E_m/c_f$. The minimum value of CRI_S is

$$\text{CRI}_S^{\text{min}} = \sqrt{\frac{c_f d_f (\sigma_f^b)^2}{8(1-c_f)E_m\tau_b\delta_b}} \quad (16)$$

Eq. (14) indicates that CRI_H decreases monotonously with increasing E_f , and reaches its minimum value when E_f reaches its maximum value of “hard matrix” case, which is $E_f = (1-c_f)E_m/c_f$. The minimum value of CRI_H is

$$\text{CRI}_H^{\text{min}} = \sqrt{\frac{c_f d_f (\sigma_f^b)^2}{8(1-c_f)E_m\tau_b\delta_b}} \quad (17)$$

which is equal to the minimum value of CRI_S in Eq. (16). However, different from CRI_S , CRI_H increases infinitely when $E_f \rightarrow 0$, without an upper bound.

Therefore, for composites with different fiber modulus E_f , there are three different cases about failure mode conversion. Correspondingly, there are three types of $\Delta K-E_f$ curves, as presented in Fig. 3, in which the fracture toughness enhancement is normalized as $\Delta \hat{K} = \Delta K \cdot \eta K_{IC} / (c_f \sigma_f^b \delta_b)$ and fiber modulus is normalized as $\hat{E}_f = c_f E_f / [(1-c_f)E_m]$. Here the parameters are $\tau_b = 6.0$ GPa, $\delta_b = 0.318$ nm, $E_m = 3.5$ GPa, $\sigma_f^b = 50$ GPa and $L = 10$ nm. For the examples presented in Fig. 3(a)–(c), the fiber volume fraction c_f is 1.5%, 0.8% and 0.3%, respectively, to show the three different types of $\Delta \hat{K} - \hat{E}_f$ curves. All the other composites with reasonable parameter values can yield similar curves to those shown in Fig. 3.

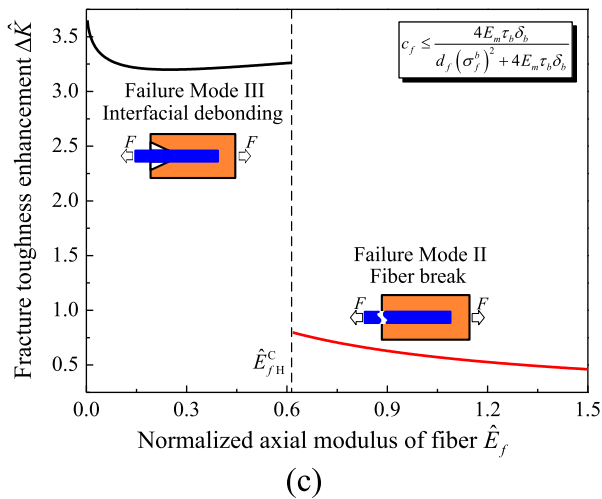
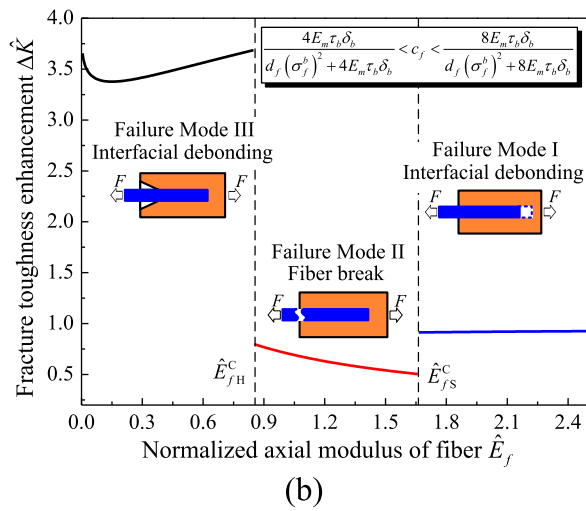
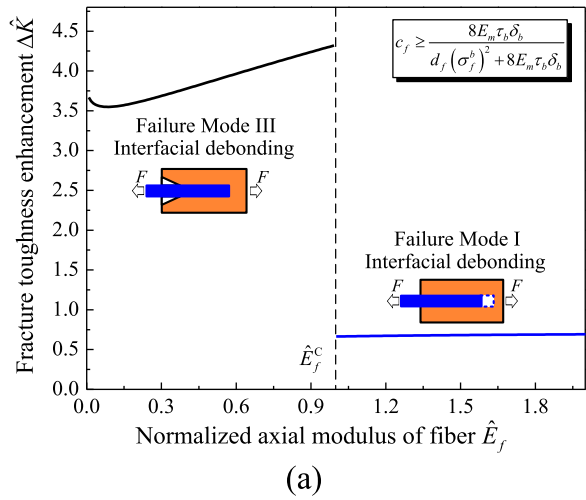


Fig. 3. Effect of fiber modulus on the fracture toughness enhancement of composites with (a) high fiber volume fraction, (b) moderate fiber volume fraction and (c) low fiber volume fraction.

Type 1: For composites with $\text{CRI}_H^{\min} = \text{CRI}_S^{\min} \geq 1$, the failure mode is always interfacial debonding, no matter how stiff or soft the fibers are. The failure mode is interfacial debonding from the outside ends of fibers (failure mode III) for the composites

reinforced by fibers with low modulus, and then with increasing fiber modulus it turns to interfacial debonding from the inside ends of fibers (failure mode I) at the critical fiber modulus $E_f^c = (1 - c_f)E_m/c_f$. The relation between the fracture toughness enhancement ΔK and the fiber modulus E_f can be obtained from Eqs. (5) and (7), and it is presented in Fig. 3(a). It is found that the fracture toughness enhancement ΔK is large when $E_f \leq E_f^c$, and drops to a low level at E_f^c and then increases slightly with increasing fiber modulus E_f .

This case happens usually for the composites with high fiber volume fraction $c_f \geq c_{f2}^c$, in which c_{f2}^c is the critical fiber volume fraction solved from $\text{CRI}_H^{\min} = \text{CRI}_S^{\min} = 1$, expressed as

$$c_{f2}^c = \frac{8E_m\tau_b\delta_b}{d_f(\sigma_f^b)^2 + 8E_m\tau_b\delta_b} \quad (18)$$

Type 2: For composites satisfying $\text{CRI}_H^{\min} = \text{CRI}_S^{\min} < 1 < \text{CRI}_S^{\text{up}}$, with the fiber modulus E_f increasing from a very low value, the failure mode first converts at the critical fiber modulus E_{fH}^c from interfacial debonding from the outside ends of fibers (failure mode III) to fiber break, and then at the critical fiber modulus E_{fS}^c it turns to interfacial debonding from the inside ends of fibers (failure mode I).

Correspondingly, the $\Delta K - E_f$ curve can be divided into three stages, as presented in Fig. 3(b). At first, the fiber has a high flexibility, the failure mode is interfacial debonding in hard matrix, and the fracture toughness enhancement ΔK is extraordinarily high. When the fiber modulus E_f reaches the critical fiber modulus E_{fH}^c , ΔK drops suddenly and the curve goes into the second stage. The drop of ΔK indicates the conversion of failure mode to fiber break. In this stage, the fracture toughness enhancement ΔK becomes extremely low and decreases with increasing E_f . If the fiber modulus E_f increases further and reaches another critical value E_{fS}^c , the fracture toughness enhancement ΔK increases suddenly, the failure mode converts to interfacial debonding, and the curve goes into the last stage. In this stage, the fracture toughness enhancement ΔK is lower than that of the first stage but higher than that of the second stage.

The two critical values of fiber modulus, E_{fS}^c and E_{fH}^c , can be derived from $\text{CRI}_S = 1$ and $\text{CRI}_H = 1$, respectively, as

$$E_{fS}^c = \frac{4\tau_b\delta_b(1 - c_f)^2 E_m^2}{d_f(c_f\sigma_f^b)^2 - 4c_f(1 - c_f)\tau_b\delta_b E_m} \quad \left(E_m < \frac{c_f}{1 - c_f} E_f\right) \quad (19)$$

$$E_{fH}^c = \frac{1}{2} \sqrt{\left(\frac{1 - c_f}{c_f}\right)^2 E_m^2 + \frac{(1 - c_f)E_m d_f (\sigma_f^b)^2}{c_f \tau_b \delta_b}} - \frac{1 - c_f}{2c_f} E_m \quad \left(E_m \geq \frac{c_f}{1 - c_f} E_f\right) \quad (20)$$

This case happens usually for the composites with moderate fiber volume fraction $c_{f1}^c < c_f < c_{f2}^c$, in which c_{f2}^c is given by Eq. (18) and c_{f1}^c is another critical fiber volume fraction solved from $\text{CRI}_S^{\text{up}} = 1$, expressed as

$$c_{f1}^c = \frac{4E_m\tau_b\delta_b}{d_f(\sigma_f^b)^2 + 4E_m\tau_b\delta_b} \quad (21)$$

Type 3: For composites satisfying $\text{CRI}_S^{\text{up}} \leq 1$, the failure mode is interfacial debonding only when the fiber modulus is lower than E_{fH}^c . With increasing fiber modulus, the failure mode changes to fiber break at $E_f = E_{fH}^c$, and different from type 2, it can never converts to interfacial debonding from the inside ends of fibers (failure mode I) even if $E_f \rightarrow \infty$. Fig. 3(c) presents the $\Delta K - E_f$ curve, from which it can be seen that the fracture toughness enhancement ΔK decreases suddenly when the failure mode converts from

Table 2

The critical fiber moduli for typical fiber reinforced composites.

Composites	E_m /GPa	d_f /nm	σ_f^b /GPa	c_{f1}^c /%	c_{f2}^c /%	c_f /%	E_{fH}^c /GPa	E_f^c /GPa	E_{fS}^c /GPa
SWCNT /epoxy	3.5	2.0	50	0.53	1.06	2.0	–	172	–
						0.7	374	–	1554
						0.3	467	–	–
SWCNT /ceramic	300	2.0	50	31.4	47.8	60	–	200	–
						40	363	–	987
						1.0	641	–	–
MWCNT /epoxy	3.5	10	30	0.3	0.6	1.0	–	347	–
						0.4	668	–	2468
						0.1	931	–	–
MWCNT /ceramic	300	10	30	20.3	33.7	50	–	300	–
						25	674	–	2901
						1.0	1136	–	–
CNF/epoxy	3.5	100	5	1.1	2.1	3	–	113	–
						1.5	183	–	540
						0.5	243	–	–
CNF/ceramic	300	100	5	47.8	64.7	70	–	129	–
						50	198	–	3265
						1.0	324	–	–

E_m : matrix modulus, d_f : fiber diameter, σ_f^b : fiber strength, c_{f1}^c and c_{f2}^c : the critical fiber volume fractions, c_f : fiber volume fraction, E_{fH}^c , E_f^c and E_{fS}^c : the critical fiber moduli.

interfacial debonding to fiber break, and maintains on a very low level and decreases with increasing fiber modulus for the fiber break failure mode. This case happens usually for the composites with low fiber volume fraction $c_f \leq c_{f1}^c$.

In summary, the $\Delta K - E_f$ function can be expressed as Eq. (22) for all the different types of composites on the assumption of $L/\sqrt{\delta_b d_f} \rightarrow \infty$.

$$\Delta K = \begin{cases} \frac{c_f \delta_b \sqrt{\frac{8E_f \tau_b \delta_b}{\pi d_f} \left(\frac{c_f E_f}{1 - c_f E_m} + 1 \right)}}{\eta K_{IC}} + \int_{\delta_b}^{\delta_{\max}} \sqrt{\frac{2c_f F_{\text{soften}}(\delta)}{\pi d_f}} d\delta & \text{if } E_f < E_{f1}^c \text{ (Interfacial debonding)} \\ \frac{c_f (\sigma_f^b)^2}{\eta K_{IC}} \sqrt{\frac{d_f \delta_b}{2\pi E_f \tau_b \left(\frac{c_f E_f}{1 - c_f E_m} + 1 \right)}} & \text{if } E_{f1}^c < E_f < E_{f2}^c \text{ (Fiber break)} \\ \frac{E_m \delta_b (1 - c_f) \sqrt{\frac{2\tau_b \delta_b}{\pi E_f d_f} \left(\frac{c_f E_f}{1 - c_f E_m} + 1 \right)}}{\eta K_{IC} \sqrt{1 - \left(\frac{1 - c_f E_m}{c_f E_f} \right)^2}} \left\{ \pi - 2 \arctan \frac{1}{\sqrt{\left(\frac{c_f E_f}{1 - c_f E_m} \right)^2 - 1}} \right\} & \text{if } E_f > E_{f2}^c \text{ (Interfacial debonding)} \end{cases} \quad (22)$$

For type 1, $E_{f1}^c = E_{f2}^c = (1 - c_f)E_m/c_f$; for type 2, $E_{f1}^c = E_{fH}^c < E_{f2}^c = E_{fS}^c$; and for type 3, $E_{f1}^c = E_{fH}^c < E_{f2}^c = \infty$.

It can be found from Fig. 3 that increasing and decreasing E_f may both increase the fracture toughness of the composites, and which way is better depends on the failure mode and fiber volume fraction. Based on the theoretical analysis, the following suggestions can be given assuming the fiber modulus can be adjusted.

- (1) If $E_f \leq (1 - c_f)E_m/c_f$ and the dominated failure mode is interfacial debonding, increasing fiber modulus E_f can increase the stiffness as well as the fracture toughness of the composites, as long as the fiber volume fraction is not too low ($c_f > c_{f1}^c$). But it is not suggested to increase E_f beyond the critical value, which is E_f^c for composites with high fiber volume fraction and E_{fH}^c for composites with moderate fiber volume fraction.
- (2) If $E_f > (1 - c_f)E_m/c_f$ and the dominated failure mode is interfacial debonding, it is not worthy to make great efforts to increase the fiber modulus if the only purpose is to

enhance fracture toughness. Because for composites dominated by this failure mode, increasing fiber modulus can only increase the fracture toughness slightly.

- (3) The failure mode of fiber break should be avoided because fracture toughness of this failure mode is much lower than those of the other two failure modes. For composites with moderate fiber volume fraction, either increasing or

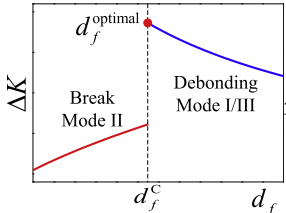
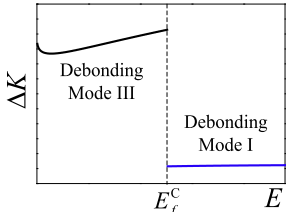
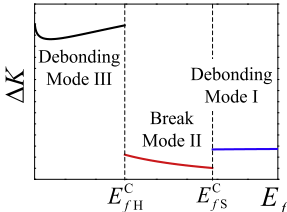
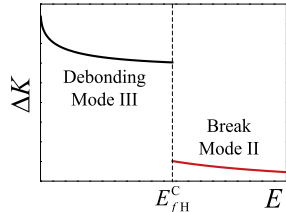
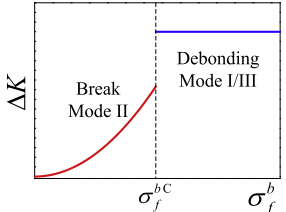
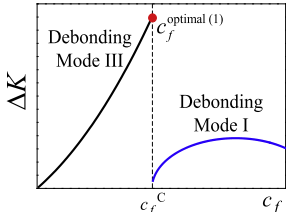
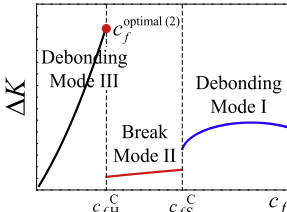
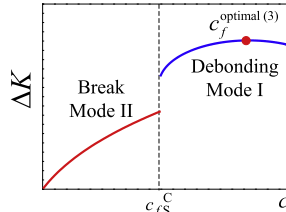
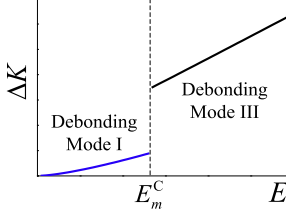
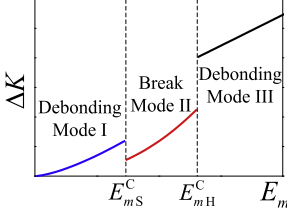
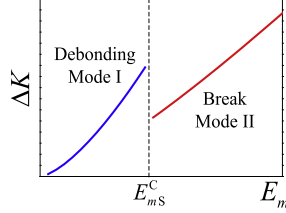
reducing fiber modulus can change the failure mode and thus increases the fracture toughness of composites. For composites with low fiber volume fraction, the only way to increase fracture toughness is to reduce the fiber modulus.

4.2. The critical fiber modulus for typical composites

For fiber reinforced composites, the critical fiber volume fraction c_{f1}^c and c_{f2}^c can be obtained from the interface properties, matrix modulus, fiber diameter and strength, according to Eqs. (21) and (18), respectively. Hence the type of composites can be determined by the fiber volume fraction c_f . For some typical CNT/CNF reinforced composites, the critical fiber volume fraction c_{f1}^c and c_{f2}^c as well as the critical fiber modulus E_{fH}^c and E_{fS}^c for different fiber volume fraction are listed in Table 2. The interface parameters τ_b and δ_b for CNT/CNF reinforced composites are determined by atomic simulation as 6.0 GPa and 0.318 nm, respectively, and all the other parameter values are within the reported ranges [1–11].

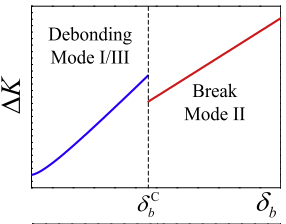
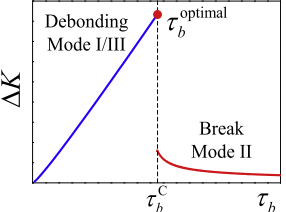
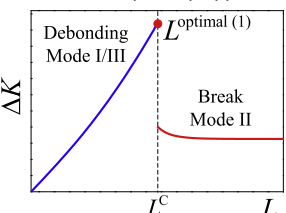
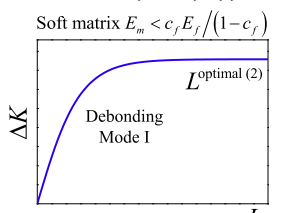
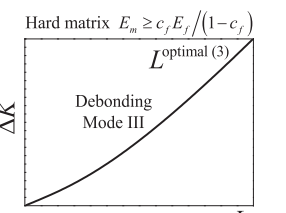
Table 3

The effects and optimal values of fiber, matrix and interface properties on fracture toughness.

Influence factor		Effect and optimal value of the factor	
Fiber	Fiber diameter d_f		$d_f^{\text{optimal}} = d_f^C = \begin{cases} \frac{4\tau_b\delta_b(1-c_f)E_m[c_fE_f+(1-c_f)E_m]}{E_f(c_f\sigma_f^b)^2} & E_m < \frac{c_f}{1-c_f}E_f \\ \frac{4\tau_b\delta_bE_f[c_fE_f+(1-c_f)E_m]}{E_m(1-c_f)(\sigma_f^b)^2} & E_m \geq \frac{c_f}{1-c_f}E_f \end{cases}$
	Fiber modulus E_f	<p>(1) $c_f \geq \frac{8E_m\tau_b\delta_b}{d_f(\sigma_f^b)^2+8E_m\tau_b\delta_b}$</p>  <p>(2) $\frac{4E_m\tau_b\delta_b}{d_f(\sigma_f^b)^2+4E_m\tau_b\delta_b} < c_f < \frac{8E_m\tau_b\delta_b}{d_f(\sigma_f^b)^2+8E_m\tau_b\delta_b}$</p>  <p>(3) $c_f \leq \frac{4E_m\tau_b\delta_b}{d_f(\sigma_f^b)^2+4E_m\tau_b\delta_b}$</p> 	$E_f^C = \frac{(1-c_f)E_m}{c_f}, E_{fH}^C = \frac{1}{2}\sqrt{\left(\frac{1-c_f}{c_f}\right)^2 E_m^2 + \frac{E_m d_f (1-c_f)(\sigma_f^b)^2}{c_f \tau_b \delta_b}} - \frac{1-c_f}{2c_f} E_m, E_{fS}^C = \frac{4\tau_b\delta_b(1-c_f)^2 E_m^2}{d_f(c_f\sigma_f^b)^2 - 4c_f(1-c_f)\tau_b\delta_b E_m}$
	Fiber strength σ_f^b		$\sigma_f^{\text{optimal}} \geq \sigma_f^{bC} = \begin{cases} \frac{(1-c_f)E_m}{c_f E_f} \sqrt{\frac{4E_f\tau_b\delta_b}{d_f} \left(\frac{c_f E_f}{(1-c_f)E_m} + 1 \right)} & E_m < \frac{c_f}{1-c_f}E_f \\ \sqrt{\frac{4E_f\tau_b\delta_b}{d_f} \left(\frac{c_f E_f}{(1-c_f)E_m} + 1 \right)} & E_m \geq \frac{c_f}{1-c_f}E_f \end{cases}$
Matrix	Fiber volume fraction c_f	<p>(1) $\sigma_f^b \geq \sqrt{8E_f\tau_b\delta_b/d_f}$</p>  <p>(2) $\sqrt{4E_f\tau_b\delta_b/d_f} < \sigma_f^b < \sqrt{8E_f\tau_b\delta_b/d_f}$</p>  <p>(3) $\sigma_f^b \leq \sqrt{4E_f\tau_b\delta_b/d_f}$</p> 	$c_f^{\text{optimal}(1)} = c_f^C = \frac{E_m}{E_m + E_f}, c_f^{\text{optimal}(2)} = c_{fH}^C = \frac{E_m[d_f(\sigma_f^b)^2 - 4E_f\tau_b\delta_b]}{4E_f^2\tau_b\delta_b + E_m[d_f(\sigma_f^b)^2 - 4E_f\tau_b\delta_b]},$ $c_f^{\text{optimal}(3)} \text{ is solved from } \frac{\partial \Delta K_{\text{debonding}}}{\partial c_f} = 0, c_{fS}^C = \frac{2E_m\tau_b\delta_b + \sqrt{(2E_m\tau_b\delta_b)^2 + 4\tau_b\delta_b d_f(E_m\sigma_f^b)^2/E_f}}{d_f(\sigma_f^b)^2 + 2E_m\tau_b\delta_b + \sqrt{(2E_m\tau_b\delta_b)^2 + 4\tau_b\delta_b d_f(E_m\sigma_f^b)^2/E_f}}$
	Matrix modulus E_m	<p>(1) $\sigma_f^b \geq \sqrt{8E_f\tau_b\delta_b/d_f}$</p>  <p>(2) $\sqrt{4E_f\tau_b\delta_b/d_f} < \sigma_f^b < \sqrt{8E_f\tau_b\delta_b/d_f}$</p>  <p>(3) $\sigma_f^b \leq \sqrt{4E_f\tau_b\delta_b/d_f}$</p> 	$E_m^C = \frac{(1-c_f)E_f}{c_f}, E_{mH}^C = \frac{4c_f\tau_b\delta_b(E_f)^2}{(1-c_f)[d_f(\sigma_f^b)^2 - 4E_f\tau_b\delta_b]}, E_{mS}^C = \frac{d_f c_f \sqrt{E_f(\sigma_f^b)^2}}{2(1-c_f)\tau_b\delta_b \sqrt{E_f} + 2(1-c_f)\sqrt{(\tau_b\delta_b)^2 E_f - d_f\tau_b\delta_b(\sigma_f^b)^2}}$ $E_m^{\text{optimal}} = +\infty$

(continued on next page)

Table 3 (continued)

Influence factor	Effect and optimal value of the factor
Interface Critical interfacial shear displacement δ_b	 $\delta_b^C = \begin{cases} \frac{E_f d_f (c_f \sigma_f^b)^2}{4 \tau_b E_m (1 - c_f) [c_f E_f + (1 - c_f) E_m]} & E_m < \frac{c_f}{1 - c_f} E_f \\ \frac{E_m d_f (1 - c_f) (\sigma_f^b)^2}{4 \tau_b E_f [c_f E_f + (1 - c_f) E_m]} & E_m \geq \frac{c_f}{1 - c_f} E_f \end{cases}$ $\delta_b^{\text{optimal}} = +\infty$
Interface strength τ_b	 $\tau_b^{\text{optimal}} = \tau_b^C = \begin{cases} \frac{E_f d_f (c_f \sigma_f^b)^2}{4 E_m \delta_b (1 - c_f) [c_f E_f + (1 - c_f) E_m]} & E_m < \frac{c_f}{1 - c_f} E_f \\ \frac{E_m d_f (1 - c_f) (\sigma_f^b)^2}{4 E_f \delta_b [c_f E_f + (1 - c_f) E_m]} & E_m \geq \frac{c_f}{1 - c_f} E_f \end{cases}$
Interface length L	<div style="display: flex; justify-content: space-around;"> <div style="text-align: center;">  <p>(1) $\tau_b \geq \frac{E_f d_f (c_f \sigma_f^b)^2}{4 E_m \delta_b (1 - c_f) [c_f E_f + (1 - c_f) E_m]}$</p> <p>$L^{\text{optimal}} (1) = L^C$</p> </div> <div style="text-align: center;">  <p>(2) $\tau_b < \frac{E_f d_f (c_f \sigma_f^b)^2}{4 E_m \delta_b (1 - c_f) [c_f E_f + (1 - c_f) E_m]}$</p> <p>Soft matrix $E_m < c_f E_f / (1 - c_f)$</p> <p>$L^{\text{optimal}} (2)$</p> </div> <div style="text-align: center;">  <p>Hard matrix $E_m \geq c_f E_f / (1 - c_f)$</p> <p>$L^{\text{optimal}} (3)$</p> </div> </div> $L^{\text{optimal}} (1) = L^C = \begin{cases} \sqrt{\frac{\delta_b E_f d_f}{4 \tau_b (1 + \frac{c_f E_f}{1 - c_f E_m})}} \ln \frac{\frac{(\sigma_f^b E_m)^2 d_f}{4 \tau_b \delta_b E_f (1 + \frac{c_f E_f}{1 - c_f E_m})} + \frac{E_m^2 d_f (c_f \sigma_f^b)^2}{4 \tau_b \delta_b (1 - c_f) [c_f E_f + (1 - c_f) E_m]} \left[\frac{c_f}{1 - c_f} - \left(\frac{E_m}{E_f} \right)^2 \right]}{\frac{c_f}{1 - c_f} E_f d_f} & E_m < \frac{c_f E_f}{1 - c_f} \\ \sqrt{\frac{\delta_b E_f d_f}{4 \tau_b (1 + \frac{c_f E_f}{1 - c_f E_m})}} \ln \frac{\frac{4 \tau_b \delta_b E_m [1 - c_f E_m - 1]}{c_f d_f} (1 - c_f) - (\sigma_f^b)^2 \left[\left(\frac{1 - c_f E_m}{c_f E_f} \right)^2 - 1 \right]}{\frac{E_m (1 - c_f)}{c_f} \left(\sqrt{\frac{4 \tau_b \delta_b}{E_f d_f} \left(1 + \frac{c_f E_f}{1 - c_f E_m} \right)} \sigma_f^b \right)} & E_m \geq \frac{c_f E_f}{1 - c_f} \end{cases}$ <p>$L^{\text{optimal}} (2) = L^{\text{optimal}} (3) = +\infty$</p>

For SWCNT reinforced composites, when the fiber volume fraction $c_f < c_{f2}^C$, the critical fiber modulus at transition to failure mode III (E_f^C or E_{fH}^C) is 300–700 GPa, close to the modulus of SWCNTs. So for these composites, increasing fiber modulus may reduce the fracture toughness significantly. However, for composites with high fiber volume fraction $c_f > c_{f2}^C$, the critical fiber modulus is less than 200 GPa, much lower than the modulus of SWCNTs. So for these composites, it is impossible to make the main failure mode become Mode III, and it is safe to increasing fiber modulus to gain higher composite stiffness as well as a little improvement in fracture toughness, as shown in Fig. 3(a).

For MWCNT reinforced composites, when the fiber volume fraction $c_f < c_{f2}^C$, the critical fiber modulus at transition to failure mode III is over 600 GPa, and even up to 1136 GPa, much higher than the modulus of MWCNTs. So the fracture toughness of MWCNT composites is far away from its optimal value, which implies that SWCNTs are more suitable to reinforce the composite materials from the view of fracture toughness enhancement if the fiber volume fraction is not very high. Coincidentally, the same conclusion has been drawn from the aspect of interwall load transfer [60]. However, for composites with high fiber volume fraction $c_f > c_{f2}^C$, the critical fiber modulus is around 300 GPa, very close to the modulus of MWCNTs. So for this case, additional attentions should be

paid to the critical values, because a little change in fiber modulus may lead tremendous change in the toughening effect of MWCNTs in their composites.

For CNFs reinforced composites, the critical fiber modulus at transition to failure mode III (E_f^C or E_{fH}^C) is on the order of 10^2 GPa, close to the modulus of CNFs. So it may dangerous to increase fiber modulus due to the probable sudden drop in composite toughness. And it should be noted that for the composites with ceramic matrix, the two critical fiber volume fractions are both much higher than fiber volume fraction in present studies, which means the present CNF/ceramic composites mostly belong to type 3 (Fig. 3(c)), and thus reducing fiber modulus is the only way to improve composite fracture toughness.

5. Other factors influencing fracture toughness

Eqs. (5) and (7) indicates that some other properties also influence the fracture toughness, including the fiber strength σ_f^b , fiber volume fraction c_f , matrix modulus E_f and the critical shear displacement δ_b . This section will investigate the effects of these factors and give the analytical optimal values of these factors based on the reasonable assumption of $L/\sqrt{\delta_b d_f} \rightarrow \infty$. For concision, the effects of these factors on the fracture toughness enhancement

ΔK are summarized in Table 3. The fiber diameter d_f and fiber stiffness E_f discussed above as well as the interface strength τ_b and interface length L studied in Refs. [35,36] are also listed in Table 3 for integrity.

As for the effect of fiber strength σ_f^b , it can be found in Eqs. (5) and (7) that ΔK increases quadratically with increase of σ_f^b when the failure mode is fiber break. However, if the failure mode is interfacial debonding, σ_f^b has no effect on ΔK , and ΔK remains a constant, which is higher than the maximal value of the other failure mode. Therefore, the optimal ΔK can be achieved as long as the failure mode is interfacial debonding, and the fiber strength σ_f^b that satisfies this failure mode condition is its optimal value, as shown in Table 3.

The effects of fiber volume fraction c_f on fracture toughness enhancement can be classified into three different types according to the fiber strength. (1) If the fiber strength is strong enough ($\sigma_f^b \geq \sqrt{8E_f\tau_b\delta_b/d_f}$), the failure mode is always interfacial debonding due to the strong fiber strength, but with increasing fiber volume fraction c_f , the failure mode changes from interfacial debonding in hard matrix (failure mode III) to that in soft matrix (failure mode I) at the critical value $c_f = E_m/(E_m + E_f)$, where ΔK reaches its optimal value. (2) If the fiber strength is moderate ($\sqrt{4E_f\tau_b\delta_b/d_f} < \sigma_f^b < \sqrt{8E_f\tau_b\delta_b/d_f}$), the failure mode can change from interfacial debonding in hard matrix (failure mode III) to fiber break with increase of fiber volume fraction c_f , and ΔK reaches its optimal value just in the transition. Then further increasing c_f can make the failure mode change to interfacial debonding in soft matrix (failure mode I), with a slight increase in ΔK . (3) For the composites with fibers weak enough ($\sigma_f^b \leq \sqrt{4E_f\tau_b\delta_b/d_f}$), the failure mode changes from fiber break to interfacial debonding in soft matrix (failure mode I) with increasing fiber volume fraction c_f . The maximal value of ΔK and optimal value of c_f can be obtained analytically in the stage of debonding mode by $\partial\Delta K_s/\partial c_f = 0$ and $\partial^2\Delta K_s/\partial c_f^2 < 0$ as listed in Table 3.

Similar to the effect of fiber volume fraction c_f , the effect of matrix modulus E_m on fracture toughness enhancement also presents in three different ways according to the fiber strength, as listed in Table 3. However, different from the effect of c_f , the fracture toughness enhancement ΔK always increases with increasing E_m . Therefore, stiffer matrix can be toughened more by fibers.

About the interface properties, interface strength τ_b and interface length L have already studied in Refs. [35,36]. But Eqs. (5) and (7) show that another interface parameter, the critical interfacial shear displacement δ_b , can also affect ΔK . So δ_b is investigated here for integrity. With increasing δ_b , the failure mode can convert from interfacial debonding to fiber break, but ΔK always increase with δ_b no matter of failure modes. So larger δ_b definitely leads to better toughening effect of fibers in composites. However, it is hardly to increase δ_b because it depends only on the type of functionalization bond at the interface.

6. Conclusions

Based on the three-level failure analysis model, the effects of fiber diameter on the fracture toughness of nanofiber/nanotube reinforced composites are investigated, and it is found that thinner reinforcing fibers do not definitely confer better fracture toughness on composites when the concept of fiber extends to nanofibers and nanotubes. With a decrease in fiber diameter, the failure mode is converted from fiber pull-out to fiber break and the fracture toughness drops suddenly during this transition. The optimal fiber diameter is that making the failure mode just in the transition, and can be estimated analytically by Eq. (10). Studies show that this

optimal fiber diameter is in the range of diameters of CNTs and CNFs, so “thinner is better” is no longer applicable for advanced nano-composites.

Besides, other influence factors, including fiber stiffness, fiber strength, fiber volume fraction, matrix modulus and the critical interfacial shear displacement are also studied, and a table with the effects of fiber, matrix and interface properties as well as their optimal values are provided, which has guiding significance for the advanced composite material design. It should be noted that the theoretical analysis and analytical solutions obtained in this study can also be extended to composites reinforced by conventional fibers, such as the widely-used carbon fibers and glass fibers.

Acknowledgements

Supports by the National Natural Science Foundation of China (Nos. 11202012 and 11472027) and the Program for New Century Excellent Talents in University (No. NCET-13-0021) are gratefully acknowledged.

References

- [1] Tibbetts GG, Lake ML, Strong KL, Rice BP. A review of the fabrication and properties of vapor-grown carbon nanofiber/polymer composites. *Compos Sci Technol* 2007;67:1709–18.
- [2] Hammel E, Tang X, Trampert M, Schmitt T, Mauthner K, Eder A, et al. Carbon nanofibers for composite applications. *Carbon* 2004;42:1153–8.
- [3] Huang ZM, Zhang YZ, Kotakic M, Ramakrishn S. A review on polymer nanofibers by electrospinning and their applications in nanocomposites. *Compos Sci Technol* 2003;63:2223–53.
- [4] Kim JS, Reneker DH. Mechanical properties of composites using ultrafine electrospun fibers. *Polym Compos* 1999;20:124–31.
- [5] Baji A, Mai YW, Wong SC, Abtahi M, Chen P. Electrospinning of polymer nanofibers: effects on oriented morphology, structures and tensile properties. *Compos Sci Technol* 2010;70:703–18.
- [6] Baughman RH, Zakhidov AA, Heer WA. Carbon nanotubes: the route toward applications. *Science* 2002;297:787–92.
- [7] Chen YL, Liu B, Wu J, Huang Y, Jiang H, Hwang KC. Mechanics of hydrogen storage in carbon nanotubes. *J Mech Phys Solids* 2008;56:3224–41.
- [8] Yin Y, Chen YL, Yin J, Huang KC. Geometric conservation laws for Y-branched carbon nanotubes. *Nanotechnology* 2006;17:1–5.
- [9] De Volder MFL, Tawfick SH, Baughman RH, Hart AJ. Carbon nanotubes: present and future commercial applications. *Science* 2013;393:535–9.
- [10] Yu MF, Files BS, Arepalli S, Ruoff RS. Tensile loading of ropes of single-wall carbon nanotubes and their mechanical properties. *Phys Rev Lett* 2000;84:5552–5.
- [11] Yu MF, Lourie O, Dyer MJ. Strength and breaking mechanism of multiwalled carbon nanotubes under tensile load. *Science* 2000;287:637–40.
- [12] Allaoui A, Bai S, Cheng H, Bai J. Mechanical and electrical properties of a MWCNT/epoxy composite. *Compos Sci Technol* 2002;62:1993–8.
- [13] Bai J, Allaoui A. Effect of the length and the aggregate size of MWNTs on the improvement efficiency of the mechanical and electrical properties of nanocomposites experimental investigation. *Composite Part A* 2003;34:689–94.
- [14] Gojny F, Wichmann M, Fiedler B, Bauhofer W, Schulte K. Influence of nano-modification on the mechanical and electrical properties of conventional fibre-reinforced composites. *Composite Part A* 2005;36:1525–35.
- [15] Zhou Y, Wu P, Cheng Z, Ingram J, Jeelani S. Improvement in electrical, thermal and mechanical properties of epoxy by filling carbon nanotubes. *Express Polym Lett* 2008;2:40–8.
- [16] Moniruzzaman M, Du FM, Romero N, Winey KI. Increased flexural modulus and strength in SWNT/epoxy composites by a new fabrication method. *Polymer* 2006;47:293–8.
- [17] Gojny FH, Wichmann MHG, Fiedler B, Schulte K. Influence of different carbon nanotubes on the mechanical properties of epoxy matrix composites—a comparative study. *Compos Sci Technol* 2005;65:2300–13.
- [18] Gojny FH, Wichmann MHG, Köpke U, Fiedler B, Schulte K. Carbon nanotube reinforced epoxy-composites: enhanced stiffness and fracture toughness at low nanotube volume fraction. *Compos Sci Technol* 2004;64:2363–71.
- [19] Yang BX, Shi JH, Pramoda KP, Goh SH. Enhancement of stiffness, strength, ductility and toughness of poly (ethylene oxide) using phenoxy-grafted multiwalled carbon nanotubes. *Nanotechnology* 2007;18:1–7. 125606.
- [20] Fiedler B, Gojny FH, Wichmann MHG, Nolte MCM, Schulte K. Fundamental aspects of nano-reinforced composites. *Compos Sci Technol* 2006;66:3115–25.
- [21] Dondero WE, Gorga RE. Morphological and mechanical properties of carbon nanotube/polymer composites via melt compounding. *J Polym Sci Pol Phys* 2006;44:864–78.
- [22] Tang LC, Wan YJ, Peng K, Pei YB, Wu LB, Chen LM, et al. Fracture toughness and electrical conductivity of epoxy composites filled with carbon nanotubes and spherical particles. *Composite Part A* 2013;45:95–101.

- [23] Ma PC, Kim JK, Tang BZ. Effects of silane functionalization on the properties of carbon nanotube/epoxy nanocomposites. *Compos Sci Technol* 2007;67: 2965–72.
- [24] Bauhofer W, Kovacs WJZ. A review and analysis of electrical percolation in carbon nanotube polymer composites. *Compos Sci Technol* 2009;69:1486–98.
- [25] Kwon SY, Kwon IM, Kim YG, Lee S, Seo YS. A large increase in the thermal conductivity of carbon nanotube/polymer composites produced by percolation phenomena. *Carbon* 2013;55:285–90.
- [26] Bozlar M, He MDL, Bai JB, Chalopin Y, Mingo YN, Volz S. Carbon nanotube microarchitectures for enhanced thermal conduction at ultralow mass fraction in polymer composites. *Adv Mater* 2010;22:1654–8.
- [27] Han ZD, Fina A. Thermal conductivity of carbon nanotubes and their polymer nanocomposites: a review. *Prog Polym Sci* 2011;36:914–44.
- [28] Chen XY, Beyerlein IJ, Brinson LC. Curved-fiber pull-out model for nanocomposites. Part 1: bonded stage formulation. *Mech Mater* 2009;41: 279–92.
- [29] Chen XY, Beyerlein IJ, Brinson LC. Curved-fiber pull-out model for nanocomposites. Part 2: interfacial debonding and sliding. *Mech Mater* 2009;41:293–307.
- [30] Chen XY, Beyerlein IJ, Brinson LC. Bridged crack models for the toughness of composites reinforced with curved nanotubes. *J Mech Phys Solids* 2011;59: 1938–52.
- [31] Pavia F, Curtin WA. Optimizing strength and toughness of nanofiber-reinforced CMCs. *J Mech Phys Solids* 2012;60:1688–702.
- [32] Li LL, Xia ZH, Curtin WA, Yang YQ. Molecular dynamics simulations of interfacial sliding in carbon-nanotube/diamond nanocomposites. *J Am Ceram Soc* 2009;92(10):2331–6.
- [33] Pavia F, Curtin WA. Interfacial sliding in carbon nanotube/diamond matrix composites. *Acta Mater* 2011;59:6700–9.
- [34] Pavia F, Curtin WA. Molecular modeling of cracks at interfaces in nanoceramic composites. *J Mech Phys Solids* 2013;61:1971–82.
- [35] Chen YL, Liu B, He XQ, Huang Y, Hwang KC. Failure analysis and the optimal toughness design of carbon nanotube-reinforced composites. *Compos Sci Technol* 2010;70:1360–7.
- [36] Chen YL, Liu B, Huang Y, Hwang KC. Fracture toughness of carbon nanotube-reinforced metal- and ceramic-matrix composites. *J Nanomater* 2011;746029: 1–9.
- [37] Tang LC, Zhang H, Han JH, Wu XP, Zhang Z. Fracture mechanisms of epoxy filled with ozone functionalized multi-wall carbon nanotubes. *Compos Sci Technol* 2011;72(1):7–13.
- [38] Tang LC, Zhang H, Wu XP, Zhang Z. A novel failure analysis of multi-walled carbon nanotubes in epoxy matrix. *Polymer* 2011;52(9):2070–4.
- [39] Lin Z, Li VC. Crack bridging in fiber reinforced cementitious composites with slip-hardening interfaces. *J Mech Phys Solids* 1997;45(5):763–87.
- [40] Fisher FT, Bradshaw RD, Brinson LC. Effects of nanotube waviness on the modulus of nanotube reinforced polymers. *Appl Phys Lett* 2002;80(24): 4647–9.
- [41] Wong SC, Baji A, Leng SW. Effect of fiber diameter on tensile properties of electrospun poly (-caprolactone). *Polymer* 2008;49:4713–22.
- [42] Arinstein A, Burman M, Gendelman O, Zussman E. Effect of supramolecular structure on polymer nanofibre elasticity. *Nat Nanotechnol* 2007;2:59–62.
- [43] Chen F, Peng XW, Li TT, Chen SL, Wu XF, Reneker DH, et al. Mechanical characterization of single high-strength electrospun polyimide nanofibres. *J Phys D Appl Phys* 2008;41(025308):1–8.
- [44] Chen SY, Hufnagel TC, Lim CT, Leong KW. Mechanical properties of single electrospun drug-encapsulated nanofibres. *Nanotechnology* 2006;17(15): 3880–91.
- [45] Dingreville R, Qu RJM, Cherkaoui M. Surface free energy and its effect on the elastic behavior of nano-sized particles, wires and films. *J Mech Phys Solids* 2005;53:1827–54.
- [46] Cox HL. The elasticity and strength of paper and other fibrous materials. *Br J Appl Phys* 1952;3(1):72–9.
- [47] Chon TW, Sun CT. Stress distributions along a short fiber in fiber reinforced plastics. *J Mater Sci* 1980;15(4):931–8.
- [48] Lawrence P. Some theoretical considerations of fiber pull-out from an elastic matrix. *J Mater Sci* 1972;7(1):1–6.
- [49] Marshall DB, Cox BN, Evans AG. The mechanics of matrix cracking in brittle-matrix fiber composites. *Acta Metall* 1985;33(11):2013–22.
- [50] Hutchinson JW, Jensen HM. Models of fiber debonding and pullout in brittle composites with friction. *Mech Mater* 1990;9:139–63.
- [51] Budiansky B, Evans AG, Hutchinson JW. Fiber-matrix debonding effects on cracking in aligned fiber ceramic composites. *Int J Solids Struct* 1995;32: 315–28.
- [52] Qian D, Dickey EC, Andrews R, Rantell T. Load transfer and deformation mechanisms in carbon nanotube-polystyrene composites. *Appl Phys Lett* 2000;76(20):2868–70.
- [53] Anderson TL. Fracture mechanics: fundamentals and applications. Boca Raton: CRC Press LLC; 1995.
- [54] Tada H, Paris PC, Irwin GR. The stress analysis of cracks handbook. 3rd ed. New York: ASME Press; 2000.
- [55] Al-Saleh MH, Sundararaj U. Review of the mechanical properties of carbon nanofiber/polymer composites. *Composite Part A* 2011;42:2126–42.
- [56] Arshad SN, Naraghi M, Chasiotis I. Strong carbon nanofibers from electrospun polyacrylonitrile. *Carbon* 2011;49:1710–9.
- [57] Feng LC, Xie N, Zhong J. Carbon nanofibers and their composites: a review of synthesizing, properties and applications. *Materials* 2014;7:3919–45.
- [58] Namat-Nasser S, Hori M. Micromechanics: overall properties of heterogeneous materials. North-holland series in applied mathematics and mechanics series. Elsevier; 1993.
- [59] Escamilla CG, Laviada RJ, Cupul CJI, Mendizábal E, Puig JE, Franco HPJ. Flexural, impact and compressive properties of a rigid-thermoplastic matrix/cellulose fiber reinforced composites. *Composites Part A* 2002;33:539–49.
- [60] Chen YL, Liu B, Hwang KC, Huang YG. A theoretical evaluation of load transfer in multi-wall carbon nanotubes. *Carbon* 2011;49(1):193–7.